Supporting Information

Gorrie et al. 10.1073/pnas.1405741111

SI Materials and Methods

Promoter Assay of Human Ubiquilin2 Gene. Three primers were synthesized: P1, 5′-ctactcgagcacggtacctctgtgatgaag-3; P2, 5′-cttagagctctgtgatttccctataactac-3′; and P3, 5′-gcttactgagctccttcttcaaagat-3′. A human BAC clone containing ubiquilin2 (*UBQLN2*) gene (RP11-431N15) was used as a template for PCR. P1 and P2 were used for amplification of the fragment for construct 1, and P1 and P3 for construct 2. The PCR products were digested with SacI and XhoI and cloned into the SacI and XhoI sites of pCAT3 vector (Promega). A molecular ratio of 3:1 for pCAT3 plasmid and pCMVβ plasmid (Clontech) was used for transfection of Neuro-2a cells. chloramphenicol acetyltransferase (CAT) assay was carried out using the CAT ELISA kit (Roche) using the manufacturer's protocols. The CAT amounts (activities) were normalized to β-galactosidase activity.

Construction of *UBQLN2* Transgene and Development of Transgenic Mice. The 7.0-kb EcoRI/KpnI fragment was isolated from the BAC clone (RP11-431N15) by restriction digestion/gel purification and cloned into plasmid vector. The 3.8-kb KpnI/BamHI fragment was PCR amplified from the BAC clone with KpnI- and BamHI-anchored primers (P4, 5′-cagtcttcatcacagaggtaccgtgc-3′ and P5, 5′-catggatcctgtatgtctgtattacctag-3′). The PCR product was digested with KpnI and BamHI, agarose gel purified, and cloned into plasmid vector. The entire 3.8-kb fragment was sequenced to exclude PCR-mediated mutations using individual plasmid clones. A c.1490C > A (p.P497H) mutation was introduced into *UBQLN2* using site-directed mutagenesis (Stratagene) using a primer (P6, 5′-gtaggcccagtcaccc**a**cataggccccatagg-3′; bold letter indicates mutation site). This 3.8-kb fragment was again sequencing verified. The entire transgene was assembled by ligation of the 7.0-kb EcoRI/KpnI fragment and 3.8-kb KpnI/BamHI fragment into pBluescript plasmid vector. The 11.8-kb transgene contained a 7.0-kb promoter and a short 5′ untranslated region, *UBQLN2* coding sequence, 1.2-kb 3′ untranslated region and a 0.6-kb fragment following the *UBQLN2* polyA signal.

The transgene was released from plasmid by restriction digestion with EcoRI and BamHI, agarose-gel purified, and used for microinjection into fertilized eggs derived from a zygote of a C57BL/6 (B6) × SJL cross. Transgenic mice were identified by PCR using multiple transgene-specific primers sets (such as hgUBQLN2-P7, 5′-caggagtagggaataatcatgggat-3′ and hgUBQLN2-P8, 5′-ggtaactcataatctgctgggaa-3′). The relative transgene copy number was estimated by PCR using transgene-specific primers (hgUBQLN2-P7/hgUBQLN2-P8) and mouse alpha-actin gene-specific primers (Mactin-F, 5′-cctcaggacgacaatcgacaatc-3′ and Mactin-R, 5′-acgagtcaatctatgtacacgt-3′) in the same PCR system.

Animal Care and Use. Animal-use protocols have been approved by the Institutional Animal Care and Use Committee of Northwestern University for this project. The mice used in this study were males, which were maintained on the B6/SJL background and were housed in pathogen-free conditions in microisolator cages in the Barrier Facilities of Northwestern University Center for Comparative Medicine. Ub^{G76V}–GFP/1 (stock no. 008111) mice (1) and control mice (B6/SJL F1 hybrids) were purchased from The Jackson Laboratory. Behavioral tests were performed in the Northwestern University Behavioral Core Facility.

Western Blot, Immunohistochemistry, and Confocal and Electron Microscopy. Western blot, immunohistochemistry, and confocal and electron microscopy were performed using previously described methods (2). Antibodies against ubiquilin2, ubiquitin, p62, FUS, TDP-43, OPTN, and β-actin were the same as those used in previous studies (3, 4). Other antibodies included those to VCP (Novus Biologicals), GFP (Molecular Probes), MAP2 (Sigma), PSMD4, also known as 19S-S5A or RPN10 (Enzo Life Science), ADRM1, also known as 19S-ADRM1 or RPN13 (ProteinTech Group), PSMA4, also known as 20S-α3, PSMA7, also known as 20S-β2, and PSMB3, also known as 20S-β3 (Biomol). Modified Bielschowsky silver stain kit (American MasterTech) was used to evaluate the presence of degenerating neurons. Cresyl violet and Luxol fast blue staining was performed to stain neurons in the dentate gyrus for cell counting. The portion of the brain containing the dentate gyrus was cut into consecutive sections (10 μm) and every fourth section (a total of three to four sections) was counted. After imaging, manual cell counting was performed using ImageJ.

Spontaneous Alternation Y-Maze Task. Spontaneous alternation performance was tested as previously described (5). Each mouse was placed in the center of the symmetrical Y maze and was allowed to explore freely through the maze during an 8-min session. The sequence and total number of arms entered was recorded. Experiments were done blind with respect to the genotype of the mice. Percentage alternation is as follows: number of triads containing entries into all three arms/maximum possible alternations (the total number of arms entered − 2) × 100.

Fear Conditioning. For delay fear conditioning, mice were trained in a Plexiglas conditioning chamber. The chamber floor had a stainless steel grid for shock delivery. During training, mice were placed one at a time in the chamber, and after a 90-s baseline period they received a single conditioned stimulus (CS; tone)/unconditioned stimulus (US; shock) pairing. Each trial consisted of a 30-s tone (3 kHz, 85 dB) followed by a brief and mild foot shock (2 s, 0.7 mA). After the shock delivery, mice were left in the chamber for 30 s. Twenty-four hours after training, each mouse was placed in the same chamber and observed for freezing behavior in the original training context. Approximately 1 h after this test of contextual fear memory, the mouse was placed in a novel chamber (plain white floor without shock grid, smaller in size) located in a different context, and after 90 s received a single 30-s tone trial to detect tone signaled fear. Fear conditioning was assessed by scoring freezing behavior with automated procedures during the 30 s CS and subsequent 30-s post-CS period (6). The mouse's moment-to-moment position in the chamber was sampled at 4 Hz, and the absence of all but respiratory movement through four consecutive frames (1 s) was scored as freezing.

Water Maze. Swimming ability was first assessed using a straight water alley containing a submerged platform; no significant differences in latency were observed between genotypes. The time and distance to reach a visible platform in the Morris water maze did not show significant differences between genotypes, suggesting an equal visual acuity, swimming ability, and motivation to reach the platform in mice of both genotypes. The basic protocol and apparatus for the hidden platform version of the water maze have been described (6). The mice were given six trials per day for 5 d (three blocks of two trials; 1-min intertrial intervals, 1-h interblock intervals). Each trial ended either when an animal climbed onto the platform or when a maximum of 60 s elapsed. At the end of training, all mice were given a probe test for 60 s

with the platform removed from the pool. The data collection and analysis were performed using a digital tracking device (2020 Plus Tracking System; HVS Image).

Electrophysiology. Transgenic and control mice were anesthetized using isoflourane and killed by decapitation. The brain was quickly removed and placed in ice-cold sucrose-rich artificial cerebrospinal fluid (ACSF) containing (in millimoles): 87 NaCl, 25 $NaHCO_3$, 25 glucose, 75 sucrose, 2.5 KCl, 1.25 NaH_2PO_4, 0.5 $CaCl_2$, 7 $MgCl_2$, 1 sodium pyruvate, and 5 μM glutathione-SH. The 400-μm horizontal slices were cut in the ventral-to-dorsal direction using a tissue slicer (Leica VT1200). Slices were then stored in ACSF (in millimoles): 125 NaCl, 25 $NaHCO_3$, 25 glucose, 2.5 KCl, 1.25 NaH_2PO_4, 2 $CaCl_2$, 1 $MgCl_2$, 1 sodium pyruvate, and 5 μM glutathione for 20 min at ∼33 °C, followed by 20 min at ∼36 °C and finally at room temperature until used for experiments. Recordings were performed in a chamber continuously perfused with oxygenated ACSF containing 2.5 mM $CaCl_2$ and 100 μM picrotoxin (Ascent Scientific). The hippocampus was visualized under a Zeiss Axioskop FS microscope using DIC infrared microscopy. A bipolar stimulating electrode (FHC) was placed in the Schaffer collateral pathway in the CA1 (cornu ammonis) region. Borosilicate glass recording electrodes containing 3M NaCl and with tip resistances of 1–2.5 MΩ were placed in CA1 stratum radiatum. Recordings were made using an Axopatch 200B amplifier and electrical stimulation was delivered using an A360 Stimulus Isolator (WPI). Field potential recordings were sampled at 10 kHz and low pass filtered at 5 kHz. The ACSF in the chamber was kept at 32.2 ± 0.2 °C throughout the experiment using a feedback temperature controller (Warner Instruments).

To induce long term potentiation (LTP) the current stimulation was set to elicit an excitatory field potential with size 40–60% of the maximum response and the baseline recording was obtained by delivering one stimulation every 15 s (0.067 Hz) for 10 min. Immediately following baseline, tetanic stimulation was applied in the form of four 1-s trains at 100 Hz with 30 s in between each train. Field potentials were then elicited and recorded every 15 s for 40 min following tetanus. For data analysis, traces were averaged in 10-min bins and the slope of the field potential was measured between 20% and 80% of its maximum amplitude. Only recordings in which the stimulation protocol successfully induced posttetanic potentiation (PTP) were further studied.

Measurement of Dendritic Spine Density. For measurements of dendritic spine size and density, Golgi staining (FD Rapid GolgiStain kit; FD Neurotechnologies) was used according to the manufacturer's instructions with some modification. Briefly, the animals were killed and the brains were immediately removed and rinsed in 0.1 M phosphate buffer. Brains were immersed in a Golgi-Cox solution. The mixture of solutions was replaced after 12 h of initial immersion and stored at room temperature in darkness for 10 d. After the immersion period in the Golgi-Cox solution, brains were transferred to a cryoprotectant solution and stored at 4 °C for 48 h in the dark before cutting. Brains were rapidly frozen with dry ice and cut in the coronal plane at ∼120-μm thickness on a cryostat. The sections were transferred onto gelatin-coated slides. Cut sections were air dried at room temperature in the dark. After drying, sections were rinsed with distilled water and were subsequently stained in a developing solution and dehydrated, cleared, and coverslipped. The molecular layer of the dentate gyrus of the dorsal and ventral hippocampal area was selected for dendritic analysis. Ten fields (5 from dorsal and 5 from ventral hippocampus) of each animal were selected by stereological program (CAST) for spine density measurement using the ImageJ program. Spine density was expressed as the number of spines per 10 μm of dendrite length.

1. Lindsten K, Menéndez-Benito V, Masucci MG, Dantuma NP (2003) A transgenic mouse model of the ubiquitin/proteasome system. *Nat Biotechnol* 21(8):897–902.
2. Deng HX, et al. (2006) Conversion to the amyotrophic lateral sclerosis phenotype is associated with intermolecular linked insoluble aggregates of SOD1 in mitochondria. *Proc Natl Acad Sci USA* 103(18):7142–7147.
3. Deng HX, et al. (2011) Differential involvement of optineurin in amyotrophic lateral sclerosis with or without SOD1 mutations. *Arch Neurol* 68(8):1057–1061.
4. Deng H-X, et al. (2011) Mutations in UBQLN2 cause dominant X-linked juvenile and adult-onset ALS and ALS/dementia. *Nature* 477(7363):211–215.
5. Ohno M, et al. (2004) BACE1 deficiency rescues memory deficits and cholinergic dysfunction in a mouse model of Alzheimer's disease. *Neuron* 41(1):27–33.
6. Ohno M, et al. (2006) Temporal memory deficits in Alzheimer's mouse models: Rescue by genetic deletion of BACE1. *Eur J Neurosci* 23(1):251–260.

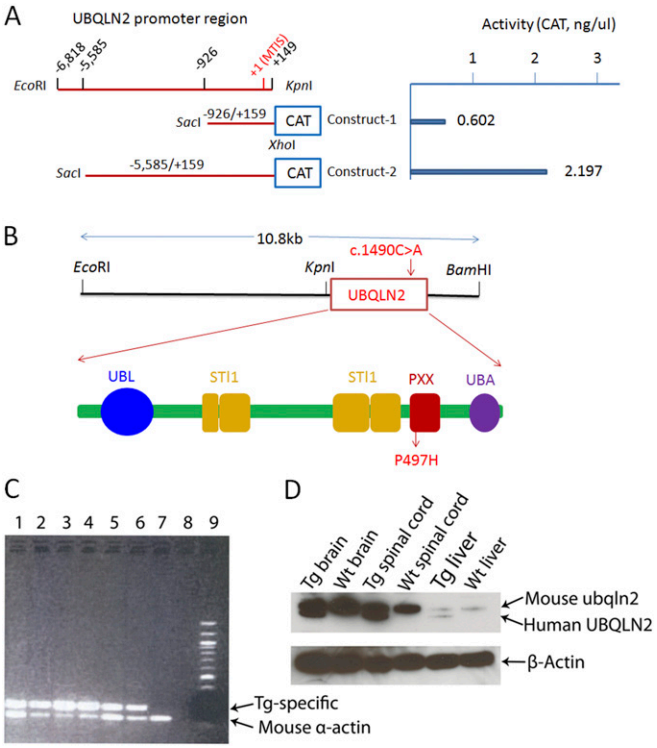

Fig. S1. Characterization of human *UBQLN2* promoter, construction of *UBQLN2* transgene, and genetic and biochemical analyses of transgenic mice. (*A*) Transient expression analysis of the chloramphenicol acetyltransferase type I (CAT) driven by the 5′-flanking region of the human *UBQLN2* gene was performed in Neuro-2a cells. (*Left*) Structures of the 7.0-kb human genomic DNA fragment upstream of the translational initiation site. Two constructs were analyzed in the present study. The numbers of the nucleotide are assigned using the major transcriptional initiation site (MTIS, +1) as a reference. The minus and plus sides indicate the upstream (5′ side) and downstream (3′ side) of the MTIS, respectively. Genomic DNA fragments were generated by PCR using SacI- and XhoI-anchored primers and a BAC clone containing the entire human UBQLN2 gene (RP11-431N15) as a template, and cloned into the SacI and XhoI sites of pCAT3 reporter vector (Promega). A molecular ratio of 3:1 for pCAT plasmid and pCMVβ plasmid (Clontech) was used for each transfection. CAT assay was carried out using the CAT ELISA kit (Roche). The CAT amounts (activities) are shown on the *Right*. The CAT activities were normalized to β-galactosidase activity. Construct 2 showed a higher promoter activity. (*B*) Schematic structure of human *UBQLN2*^{P497H} transgene. The 7.0-kb EcoRI/KpnI fragment was isolated from the BAC clone (RP11-431N15) by restriction digestion/gel purification and cloned into plasmid vector. The 3.8-kb KpnI/BamHI fragment was PCR amplified from the BAC clone with KpnI- and BamHI-anchored primers and cloned into plasmid vector. The entire 3.8-kb fragment was sequenced to exclude PCR-mediated mutations. A c.1490C > A (p.P497H) mutation was introduced into *UBQLN2* using site-directed mutagenesis (Stratagene). This 3.8-kb fragment was again sequencing verified. The entire transgene was assembled by ligation of the 7.0-kb EcoRI/KpnI fragment and 3.8-kb KpnI/BamHI fragment into pBluescript plasmid vector. (*C*) Transgenic founder tail genomic DNA was genotyped using two sets of primers simultaneously by PCR. Human *UBQLN2*-specific primers were used to detect the *UBQLN2*^{P497H} transgene. Mouse alpha-actin primers for amplification of alpha-actin genomic DNA were used as an internal control. Six representative *UBQLN2* transgenic founders are shown to be positive for the human *UBQLN2*^{P497H} transgene (lanes 1–6). A DNA sample from a nontransgenic mouse was used as a negative control (lane 7). A blank PCR control is shown in lane 8. Lane 9 is a DNA size marker. A stronger transgenic-specific band and a weaker mouse α-actin band suggests a relatively higher copy number of the transgene due to competition of two sets of primers during the PCR in the same reaction system, as shown in lane 3. (*D*) Western blot analysis of the transgene expression at protein level. Homogenates of the brain, spinal cord, and liver from the transgenic (Tg) line with the highest copy number and a male nontransgenic (wild-type, WT) mouse at the age of 30 d were blotted with the ubiquilin2-N antibody. Mouse endogenous ubqln2 and human UBQLN2 are polypeptides of 638 and 624 amino acids, respectively. The human UBQLN2 expression levels are similar to the mouse endogenous ubqln2 in the brain, spinal cord, and liver. The expression profiles of the transgene and mouse endogenous ubqln2 are similar. UBQLN2 and mouse ubqln2 have much higher expression in the brain and spinal cord than in the liver.

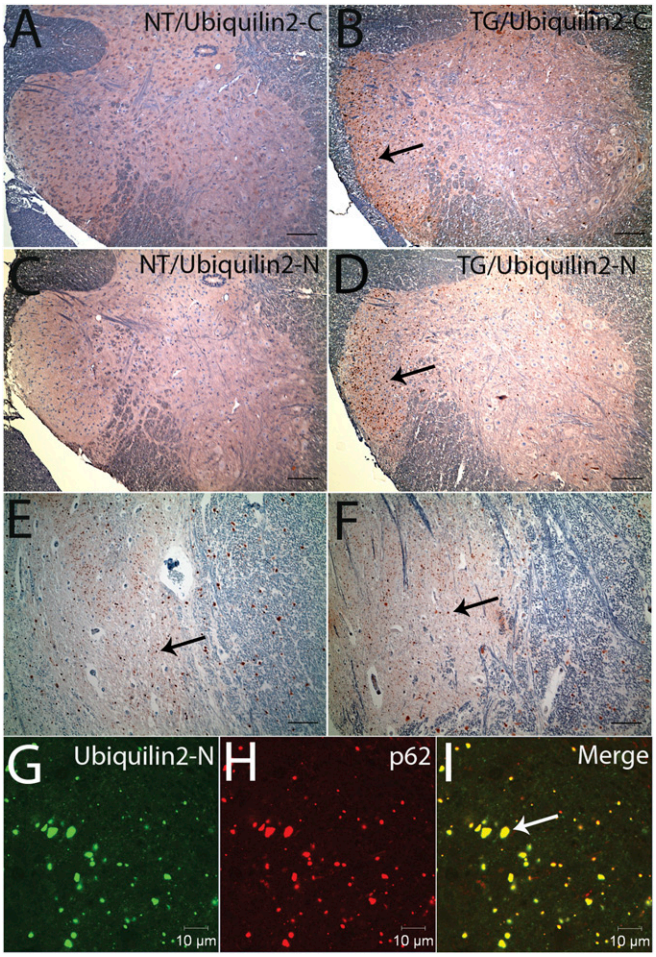

Fig. S2. Ubiquilin2 pathology in the spinal cord of the transgenic mice. (*A*–*F*) Immunohistochemistry with the ubiquilin2 antibodies (ubiquilin2-C and ubiquilin2-N) was performed on the spinal cord sections from an 11-mo-old *UBQLN2*^{P497H} transgenic mouse (*B* and *D*), an age-matched nontransgenic male mouse (*A* and *C*), and a patient with *UBQLN2*^{P506T} mutation (*E* and *F*). (*G* and *H*) Confocal microscopy was performed with antibodies to ubiquilin2 (ubiquilin2-N, green) and p62 (red) using the spinal cord sections from an 11-mo-old *UBQLN2*^{P497H} transgenic mouse. Small ubiquilin2-positve inclusions were predominantly located in the lamina II of the dorsal horns (*B* and *D*). The distribution of these small inclusions in the transgenic mouse is similar to that in the patient with the *UBQLN2*^{P506T} mutation (*E* and *F*). The ubiquilin2-positve inclusions are also p62-positive (*G*–*I*). Representative small ubiquilin2-positive inclusions in the lamina II are indicated by arrows. (Scale bars: *A*–*F*, 200 μm.)

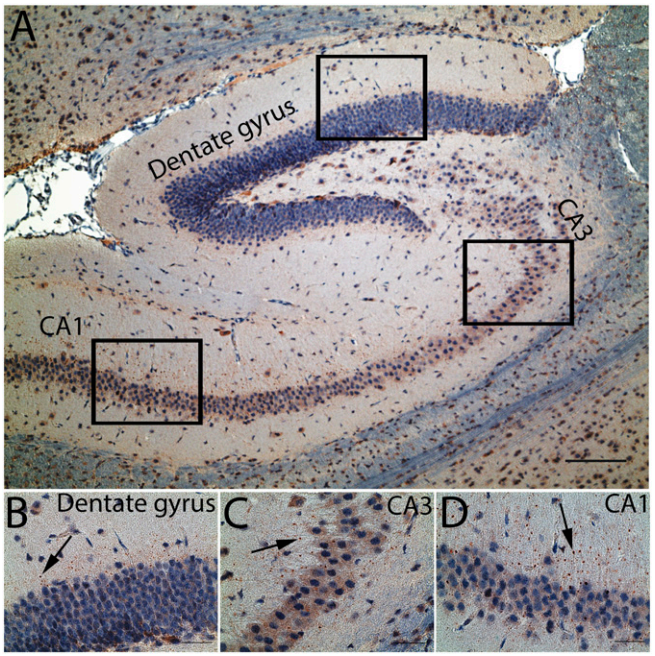

Fig. S3. Early ubiquilin2 pathology in transgenic mice. Immunohistochemistry with the ubiquilin2-N antibody was performed using the brain sections from a *UBQLN2*^{P497H} transgenic mouse of 30 d. (*A*) An overall lower power image shows early ubiquilin2-positive aggregates in the hippocampus. (*B–D*) Higher power images from the boxed areas: dentate gyrus (*B*), CA3 (*C*), and CA1 (*D*). Arrows indicate the representative small inclusions. (Scale bars: *A*, 200 μm; *B–D*, 50 μm.)

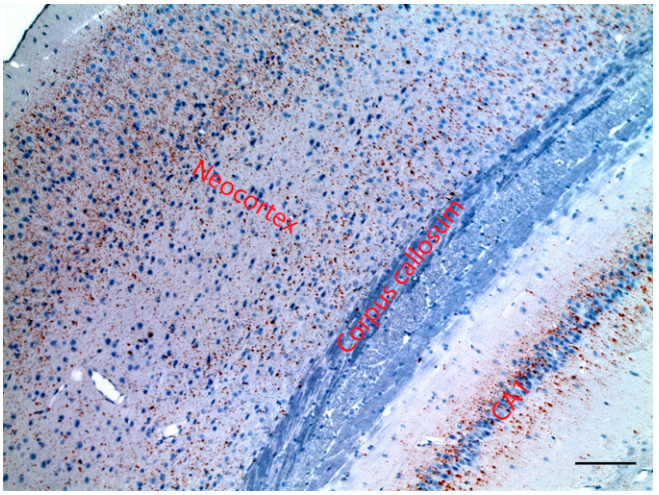

Fig. S4. Ubiquilin2 pathology in the temporal lobe of the transgenic mice. Ubiquilin2 pathology of the temporal lobe in a 15-mo-old transgenic mouse is shown in a low power image. In addition to CA1, ubiquilin2 aggregates are predominantly located in the layer II and III in the neocortex, but not in the corpus callosum. (Scale bar: 200 μm.)

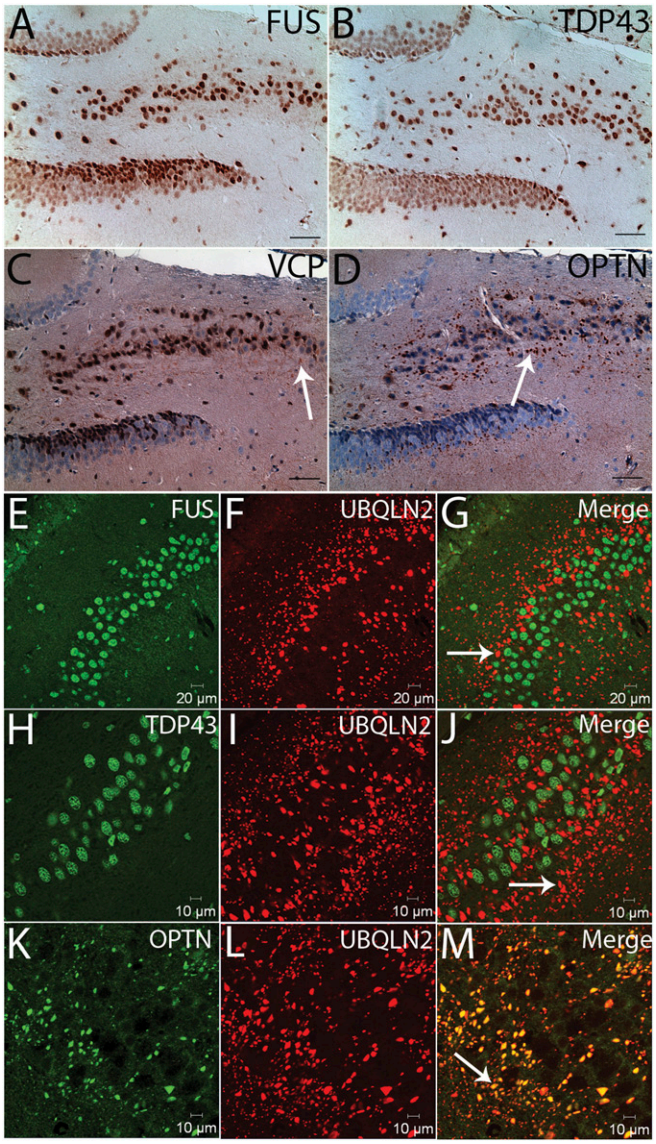

Fig. S5. ALS- and frontotemporal dementia (FTD)-associated proteins in transgenic mice. Immonohistochemtry (*A–D*) and confocal microscopy (*E–M*) were performed on hippocampal sections using antibodies to FUS, TDP43, VCP, OPTN, and ubiquilin2. Relatively weak VCP- and strong OPTN-immunoreactive aggregates were present in the hippocampus (*C* and *D*, indicated by arrows). OPTN was colocalized with ubiquilin2 in the aggregates (*K–M*, indicated by arrow in *M*). For confocal microscopy (*E–M*), representative aggregates in CA3 are shown. Hematoxylin was not used for FUS (*A*) and TDP43 (*B*) immunohistochemistry to avoid masking nuclear staining of these two proteins.

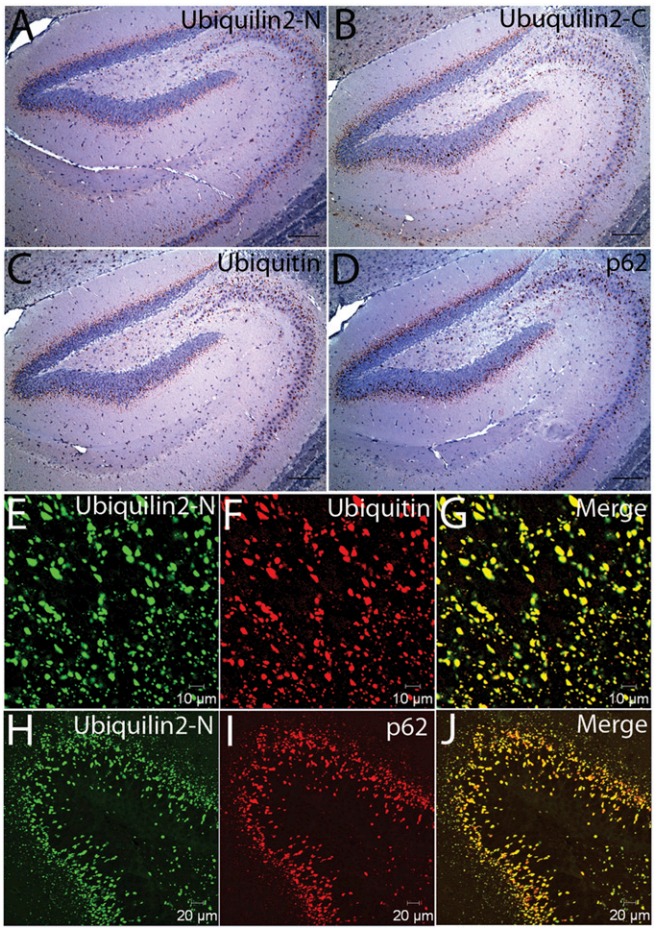

Fig. S6. Colocalization of ubiquilin2, ubiquitin, and p62 in the protein aggregates. Immonohistochemtry (*A–D*) and confocal microscopy (*E–J*) were performed on hippocampal sections of 3-mo-old (*A–D*) and 20-mo-old (*E–J*) transgenic mice using antibodies to ubiquilin2 (ubiquilin2-C and ubiquilin2-N), ubiquitin, and p62. In addition to ubiquilin2 (*A* and *B*), these aggregates are also immunoreactive to ubiquitin (*C*) and p62 (*D*). Colocalization of ubiquilin2 with ubiquitin (*E–G*, CA3) and p62 (*H–J*, dentate gyrus) is shown by confocal microscopy (*E–J*).

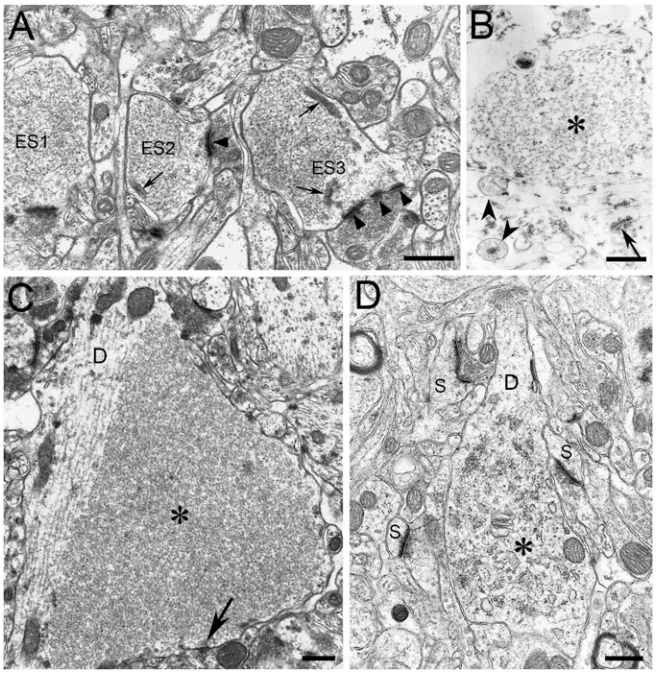

Fig. S7. Protein aggregates in dendritic stems and spines. Electron microscopy was performed using the frontal cortex and the hippocampus of a 15-mo-old transgenic mouse (*A*, *C*, and *D*) and layers I-II of the frontal cortex of an ALS/dementia patient with *UBQLN2*^{P506T} mutation (*B*). Representative electron micrographs from the frontal cortex (*A* and *D*) and hippocampal stratum oriens (*C*) of the transgenic mouse, and a presumed dendrite at the layer I-II transition of the frontal cortex of the patient (*B*) are shown. (*A*) Profiles labeled enlarged spines (ES) ES1–3 belong to three spines that likely arose from the same dendritic trunk running in another plane of section. Spine apparatus (arrows) and synaptic junctions (arrowheads) are indicated. (*B*) Granulofibrillar precipitate in a dendrite from the frontal cortex of the ALS/dementia patient is labeled by an asterisk. Despite the advanced state of autolysis, a synaptic junction (arrow) and two small mitochondrial profiles (arrowhead) are recognizable. (*C*) Large granulofibrillar inclusion (asterisk) occupies the belly-like outbulging of a small dendrite (D). A representative axodendritic synapse is indicated by an arrow. (*D*) The enlarged portion of a thin dendrite (D) contains granulofibrillar material interspersed with smooth-surfaced vesicles (asterisk) and other dendritic organelles (unlabeled). Synapse-bearing dendritic spines (S) with apparently normal fine structure are shown. (Scale bars: 0.5 μm.)

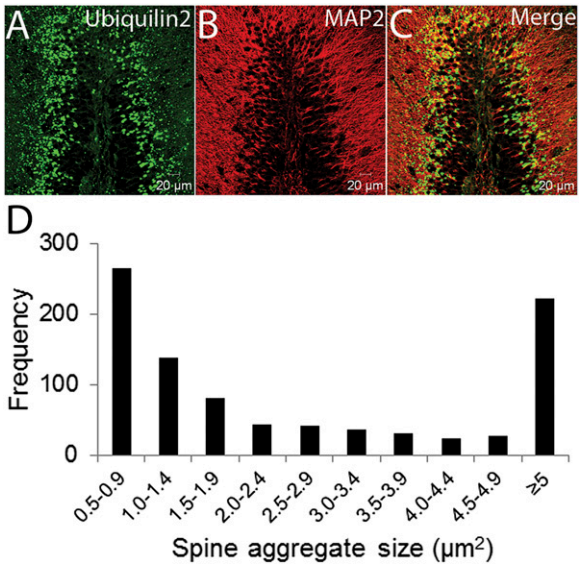

Fig. S8. Dendritic pathology. (*A*–*C*) Colocalization of ubiquilin2 with the dendritic marker (MAP2) in the dentate gyrus. (*D*) Frequency distribution of dendritic aggregates in the dentate gyrus was estimated in a representative section using ImageJ.

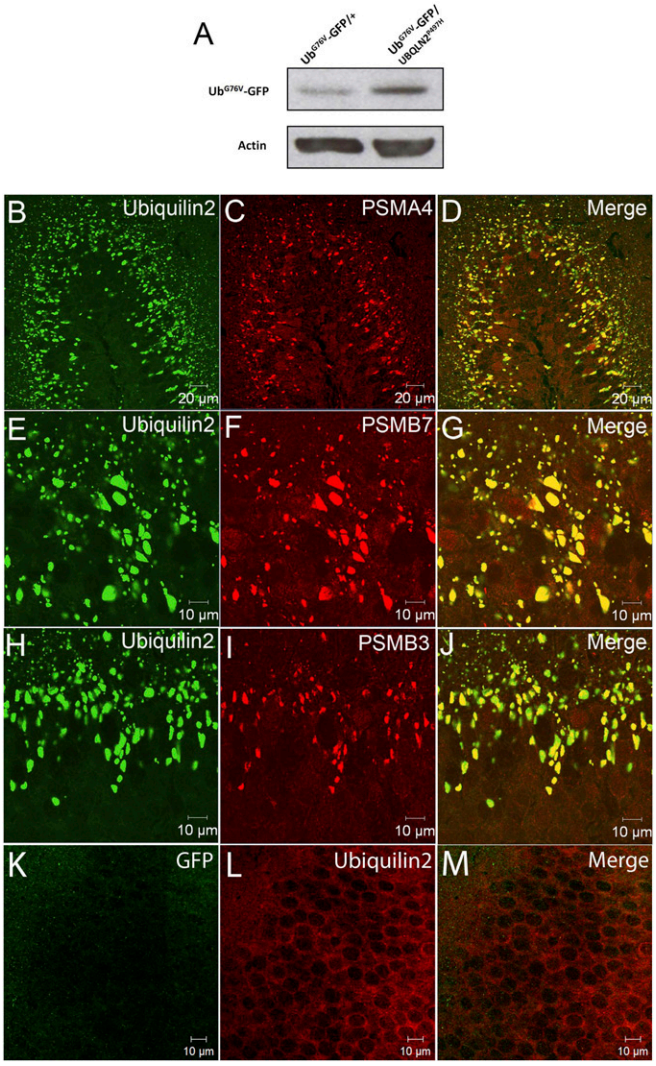

Fig. S9. Increased accumulation of Ub^{G76V}–GFP and colocalization of proteasome subunits with ubiquilin2 in protein aggregates of the *UBQLN2*^{P497H}/*Ub*^{G76V}–*GFP* double transgenic mice. (*A*) Whole brain homogenates (20 μg of total protein) from *Ub*^{G76V}–*GFP* single transgenic and *Ub*^{G76V}–*GFP*/*UBQLN2*^{P497H} double transgenic mice were blotted using antibodies against GFP and β-actin. Increased accumulation of Ub^{G76V}–GFP is shown in *Ub*^{G76V}–*GFP*/*UBQLN2*^{P497H} double transgenic mice. (*B–J*) Colocalization of proteasome subunits and ubiquilin2 in the protein aggregates. Confocal microscopy was performed on the hippocampal sections of the *UBQLN2*^{P497H}/*Ub*^{G76V}–*GFP* double transgenic mice using antibodies to ubiquilin2 and proteasome subunits as indicated. Images from dentate gyrus (*B–D* and *H–J*) and CA3 (*E–G*) are shown. No accumulation of GFP or ubiquilin2 in aggregates was seen in *Ub*^{G76V}–*GFP* single transgenic control mice (*K–L*).

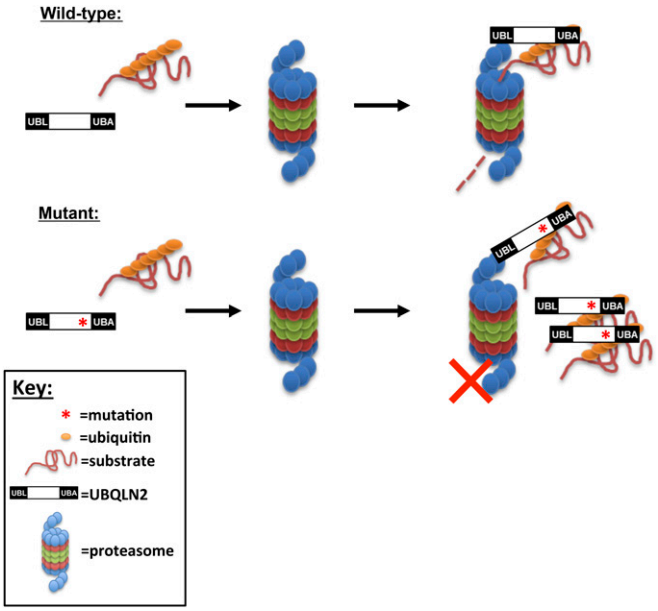

Fig. S10. Schematic model depicting an interplay between aggregate formation and ubiquitin–proteasome system (UPS) failure. Ubiquitinated substrates and related proteins, such as ubiquilin2, form functional protein complexes with the proteasomes for the clearance of ubiquitinated substrates. However, if the ubiquitinated substrates cannot be effectively cleared by the proteasomes due to genetic and/or posttranslational defects, the proteasomes would not be able to degrade other ubiquitinated substrates, thus leading to functional blockage of the UPS. In addition, the binding of UBL domain of the mutant ubiquilin2 to proteasomes would effectively prevent other UBL-containing proteins or ubiquitinated substrates from binding to the proteasomes, therefore further impairing the UPS function. Functional blockage of the UPS in turn leads to accumulation of more ubiquitinated substrates, generation of more aggregates, and further decline of the UPS. Thus, it is conceivable that if this positive-feedback cycle continues, the aggregates would increase in number and size over time, and be observed as a pathological hallmark in diseased tissues. UBA, ubiquitin-associated domain; UBL, ubiquitin-like domain.